

stereotaxic apparatus by using a ring glued to the sclera. Stability of eye position was confirmed by monitoring RF positions with a fixed reference electrode through each experiment.

Optical imaging. The exposed brain surface was illuminated with light at 610 nm (interference filter, Oriel, 30 nm). Drifting gratings (1 cycle deg⁻¹, 1 Hz) were presented at each of eight orientations spanning 180°, filling the animal's visual space. For each orientation, video images of the brain surface (8 mm × 5 mm) were digitized and accumulated at video rates (Imager 2001 system from Optical Imaging, with Bischke CCD-6012P camera and Matrox IM-640 imaging board; imager was controlled by VDAQ software and images were analysed by using TVMIX as well as custom software). Each accumulated image was divided by the corresponding image at the orthogonal orientation to correct for nonspecific stimulus-driven changes in cortical reflectivity, and the resultant image was band-pass filtered by convolving with kernel of 2 gaussians, smoothing at 12 μm and high pass at 750 μm radius. The set of all filtered orientation difference images was combined vectorially, pixel by pixel, to calculate the strength and preferred orientation of the resultant optical signal. The computed resultant orientation value at each point is shown in the polar plot (Fig. 1a).

Electrophysiology. All RFs were multi-unit and, except where mentioned otherwise, were obtained within the first 300 μm (typically within the first 150 μm) of the cortical surface. For automated maps of RF pairs (Fig 1a–c), simultaneous grid maps were obtained for both RFs of a pair (site 1 is the reference site in Fig 1a–c) by using a computer-generated visual stimulus that consisted of a single test bar, flashed in pseudo-random sequence over an 8 × 8 grid of points spanning both RFs in visual space. For hand-mapped units, RF boundaries (and orientation preferences) were mapped with respect to the RF at a fixed reference electrode, by using a hand-held visual stimulator. RFs were plotted in a 'blind' procedure, where the person plotting RF boundaries was unaware of the cortical locations of recording sites. At each recording site, both the reference RF and the new RF were plotted on a fresh sheet of paper. This was done both to correct continually for any residual drift in eye position and to avoid being influenced by existing boundaries of either the reference RF or other RFs. (This process was followed for the data shown in Fig. 1d, and for 75 of the data points in Fig. 2. Earlier measurements were also made with respect to a reference RF, but not 'blind'. The results of these earlier measurements were statistically indistinguishable from the data obtained blind, and have been combined, therefore, in the population data, to give 70 of the 145 points in Fig. 2.) In quantitative analyses (Fig. 2), we used hand-mapped values of orientation preference. In cortical regions away from orientation singularities, these values differed from optically imaged values by less than 10° (r.m.s.) and the quantitative analyses with optically mapped orientation preferences gave results that were statistically indistinguishable from the results with hand-mapped values (see supplementary information). In a separate set of experiments, we measured the scatter in RF position and size in vertical penetrations. We measured RFs (again, with a fixed reference RF) at 50 μm intervals along penetrations down to 500 μm, at 24 sites in four experiments (see Fig. 1f for results).

Monte Carlo simulations. (1) To test against null hypothesis of linear map plus scatter, for each experiment we obtained the best fit for the linear transformation (magnification plus rotation) that mapped cortical coordinates on to experimentally obtained RF centres, by minimizing the sum of squares of residual 'scatter' in RF position. Simulated RF positions were then generated for (measured) cortical positions at the best-fit linear map from cortex plus random scatter (two-dimensional gaussian, s.d. = r.m.s. minimal scatter). (2) Effect of uncertainty in experimental values: for each experiment, Monte Carlo simulations started with real data and added scatter in cortical position (two-dimensional gaussian, radius 25 μm) and in RF position (0.1 × RF size; see Fig. 1f legend).

Two-dimensional map of distorted visuotopy (Fig. 3). The grid in visual space (Fig. 3c) was constructed as follows: for the set of recordings shown (Fig. 3a,c), average local cortical magnifications were measured and the change in this average value along the anteroposterior axis was determined (1.7:1, anterior:posterior). The grid was then constructed so that the size of grid elements in each row increased in a geometric progression (factor = 1.012) so as to give a final element size of 1.7 times the initial element size at the end of the sequence of grid rows. The mapping transform for RF centres was calculated as follows: for each recording site, the set of nearest-neighbour recording sites was identified; these vertices were connected to construct the set of nearest-

neighbour triangles tessellating the cortical surface. The vector displacement required to map each triangle vertex (electrode recording site) to its corresponding RF centre was calculated and the projections of the cortical triangles on visual space were determined. The inverse of this transform was then used to map an image of the grid in visual space back to the cortical surface. The points in the interior of each triangle in visual space were mapped by the reverse affine transform back to the cortical surface, carrying with them included segments of the visual grid. The local areal compression factor (deg²mm⁻²) was then calculated as follows: for each point on a regular grid on the cortex, the square defined by the nearest neighbouring lattice points was projected back on visual space, the ratio of the (transformed) square in visual space to the square on cortex was calculated, and the average subtracted.

Gradient of orientation. For the two-dimensional surface defined by orientation values on the cortex, the local tangent was calculated (deg per 100 μm of cortex); Fig. 3d shows the magnitude of this gradient vector. To calculate cross-correlation values, this scalar magnitude was multiplied, pixel by pixel, by the areal compression factor, and averaged over the area of the transformed grid.

Received 6 January; accepted 14 April 1997.

- Hubel, D. H. & Wiesel, T. N. Sequence regularity and geometry of orientation columns in the monkey striate cortex. *J. Comp. Neurol.* **158**, 267–294 (1974).
- Ts'o, D. Y., Frostig, R. D., Lieke, E. E. & Grinvald, A. Functional organization of primate visual cortex revealed by high resolution optical imaging. *Science* **249**, 417–420 (1990).
- Blasdel, G. G. & Salama, G. Voltage-sensitive dyes reveal a modular organization in monkey striate cortex. *Nature* **321**, 579–585 (1986).
- Bonhoeffer, T. & Grinvald, A. Iso-orientation domains in cat visual cortex are arranged in pinwheel-like patterns. *Nature* **353**, 429–431 (1991).
- Talbot, S. A. & Marshall, W. H. Physiological studies on neural mechanisms of visual localization and discrimination. *Am. J. Ophthalmol.* **24**, 1255–1263 (1941).
- Daniel, P. M. & Whitteridge, D. The representation of the visual field on the cerebral cortex in monkeys. *J. Physiol. (Lond.)* **159**, 203–221 (1961).
- Hubel, D. H. & Wiesel, T. N. Uniformity of monkey striate cortex: a parallel relationship between field size, scatter, and magnification factor. *J. Comp. Neurol.* **158**, 295–302 (1974).
- Grinvald, A., Lieke, E. E., Frostig, R. D., Gilbert, C. D. & Wiesel, T. N. Functional architecture of cortex revealed by optical imaging of intrinsic signals. *Nature* **324**, 361–364 (1986).
- Frostig, R. D., Lieke, E. E., Ts'o, D. Y. & Grinvald, A. Cortical functional architecture and local coupling between neuronal activity and the microcirculation revealed by in vivo high resolution optical imaging of intrinsic signals. *Proc. Natl Acad. Sci. USA* **87**, 6082–6086 (1990).
- Motter, B. C. Focal attention produces spatially selective processing in visual cortical areas V1, V2, and V4 in the presence of competing stimuli. *J. Neurophysiol.* **70**, 909–919 (1993).
- Pettet, M. W. & Gilbert, C. D. Dynamic changes in receptive-field size in cat primary visual cortex. *Proc. Natl Acad. Sci. USA* **89**, 8366–8370 (1992).
- Das, A. & Gilbert, C. D. Receptive field expansion in adult visual cortex is linked to dynamic changes in strength of cortical connections. *J. Neurophysiol.* **74**, 779–792 (1995).
- Durbin, R. & Mitchison, G. A dimension reduction framework for understanding cortical maps. *Nature* **343**, 644–647 (1990).

Supplementary information is available on Nature's World-Wide Web site (<http://www.nature.com>) or as paper copy from Mary Sheehan at the London editorial office of Nature.

Acknowledgements. This work was supported by a grant from the NSF.

Correspondence and requests for materials should be addressed to C.D.G. (e-mail: gilbert@rockvax.rockefeller.edu).

GABA in the mammalian suprachiasmatic nucleus and its role in diurnal rhythmicity

Shlomo Wagner, Mona Castel*, Harold Gainer† & Yosef Yarom

Departments of Neurobiology, and *Cell and Animal Biology, Institute of Life Sciences, Hebrew University, Jerusalem 91904, Israel

† Laboratory of Neurochemistry, National Institutes of Health, NINDS, Bethesda, Maryland 20892, USA

Mammals manifest circadian behaviour timed by an endogenous clock in the hypothalamic suprachiasmatic nucleus (SCN)¹. Considerable progress has been made in identifying the molecular basis of the circadian clock^{2,3}, but the mechanisms by which it is translated into cyclic firing activity, high during the day and low at

night, are still poorly understood. GABA (γ -aminobutyric acid), a common inhibitory neurotransmitter in the central nervous system, is particularly densely distributed within the SCN, where it is located in the majority of neuronal somata^{4,5} and synaptic terminals^{6,7}. Using an *in vitro* brain-slice technique, we have now studied the effect of bath-applied GABA on adult SCN neurons at various times of the day. We find that GABA acts as an inhibitory neurotransmitter at night, decreasing the firing frequency; but during the day GABA acts as an excitatory neurotransmitter, increasing the firing frequency. We show that this dual effect, which is mediated by GABA_A receptors, may be attributed to an oscillation in intracellular chloride concentration. A likely explanation is that the amplitude of the oscillation in firing rate, displayed by individual neurons, is amplified by the dual effect of GABA in the SCN's GABAergic network.

There is considerable evidence indicating that GABA plays a pivotal role in circadian time-keeping, which is regulated by the firing rate of neurons in the SCN. First, there is extensive GABAergic innervation of the SCN (Fig. 1a, b)⁴⁻⁹. Moreover, cultured slice explants of the SCN, in which virtually all extrinsic inputs have degenerated, nevertheless retain a rich intrinsic GABAergic component (Fig. 1b)¹⁰. The concept of GABAergic network within the SCN appears to be supported by further observations: in freshly prepared SCN slices, 62% of the bicuculline-sensitive synaptic potentials are blocked by tetrodotoxin (TTX) ($n = 3$; results not shown), whereas the mean amplitude decreases by only 40% (the amplitudes of the synaptic potentials show a quantal distribution and only the higher peaks are abolished by TTX) indicating that the presynaptic cells existed within the slice; direct stimulation of SCN neurons with glutamate gives rise to GABAergic synaptic potentials in other SCN neurons^{11,12}; and dissociated SCN neurons communicate with each other solely via GABAergic synapses¹³. Thus, it appears that the SCN is composed of a functional, densely packed GABAergic network. Second, GABA and GABA agonists can phase-shift the circadian clock¹⁴, whereas GABA antagonists block both drug- and light-induced phase-shifts¹⁵. Third, mice devoid of prion protein, revealing weakened GABAergic synapses¹⁶, also have altered circadian rhythms^{17,18}.

To investigate the role of GABA in generating circadian behaviour and resetting the circadian clock, we studied the physiological effect of this neurotransmitter on SCN neurons. Using freshly prepared hypothalamic slices we measured, extracellularly, the effect of bath-applied GABA on the firing rate of neurons in the SCN. The circadian rhythm of firing rate of SCN neurons is well documented, the rate being high (8–10 Hz) during the day and low (2–4 Hz) at night^{19,20}. During the day, GABA at concentrations of 50–500 μ M reversibly increases the firing rate of SCN neurons (Fig. 2a), but at night GABA causes a reversible decrease in firing rate (Fig. 2b). Both the increase and decrease in firing rate are dose-dependent (Fig. 2c, d). Up to a concentration of 500 μ M, a monotonic relationship between the change in firing rate and the GABA concentration was usually observed. Both excitation (Fig. 2e) and inhibition (Fig. 2f) were blocked by picrotoxin or bicuculline, suggesting that both responses are mediated by GABA_A receptors, known to be coupled to chloride channels. Occasionally, the presence of the blocker itself has a reverse effect on the spontaneous firing: in 63% of the cases, where GABA increases the firing rate, bicuculline decreases it ($n = 8$) and vice versa ($n = 16$). The distribution of the responses (Fig. 2g) shows that during the day most of the neurons (71%) were excited by GABA application, whereas during the night most of the neurons (56%) were inhibited.

The effect of GABA on the activity of SCN neurons has been studied by several groups²¹⁻²³, showing that the most common response is a decrease in firing rate. In these studies, the excitatory response to GABA could have been masked by the use of high chloride concentrations in the extracellular pipette, which enforce inwardly directed chloride currents.

To reveal the mechanism by which the inhibitory neurotransmitter GABA acts as an excitatory agent, we used whole-cell patch recording to analyse the voltage across the membrane and its responses to current pulses before and during GABA application. In all neurons tested, GABA (100 μ M) increased the membrane conductance up to nine-fold (3.6 ± 2.7 nS, mean \pm s.d., $n = 41$), independently of the time of the day ($P > 0.3$ unpaired *t*-test; Fig. 3e). This response was accompanied by a change in membrane potential which was correlated with the chloride concentration in the patch pipette ($[Cl^-]_p$). When low $[Cl^-]_p$ was used (2 mM),

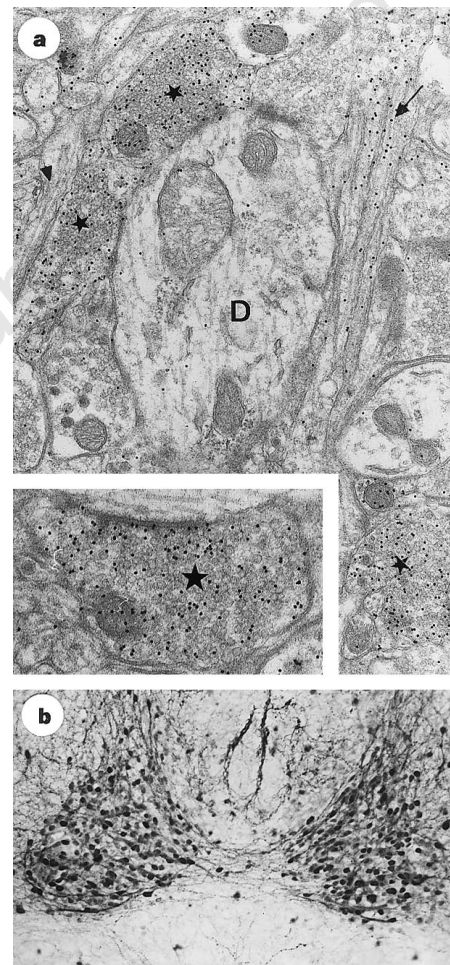


Figure 1 Immunocytochemical evidence for the extensive GABAergic innervation in the rat SCN. **a**, A typical field in the neuropil of the SCN, after post-embedding immunogold labelling of the GABA antigen. A large unlabelled proximal dendrite (D) is seen, onto which two GABA-immunoreactive terminals (asterisk) and two unlabelled terminals impinge. At the lower right part of the field is another labelled axo-dendritic GABAergic terminal (asterisk). At the upper right the concentration of gold particles (arrow) indicates a GABAergic neurite; an unlabelled neurite is seen at the upper left (arrowhead). Inset (lower left) is a larger magnification of a GABAergic terminal (large asterisk); note the gold particles are primarily over synaptic vesicles and mitochondria. Counts from our electron micrographs, derived from multiple levels within the SCN, showed that 40–70% of synaptic terminals per field were GABA-immunoreactive. **b**, Extensive GABA immunoreactivity in 3-week-old slice explant culture of the SCN. Note the numerous GABA-immunoreactive somata throughout the bilateral SCN, embedded in a dense web of immunoreactive processes. This GABAergic innervation is assumed to be of local origin, because the isolated explant retains few, if any, extrinsic GABAergic inputs. However, possible synaptic reorganization *in vitro* should be taken into account. Magnifications: **a**, $\times 20,500$; inset, $\times 40,000$; **b**, $\times 250$.

GABA induced hyperpolarization of up to 20 mV (Fig. 3a). In contrast, using 25 mM $[Cl^-]_p$ induced depolarization of the same magnitude (Fig. 3b). As with the firing rate, the voltage response to GABA was blocked by bicuculline (not shown). This, in addition to the dependence of the voltage response on $[Cl^-]_p$, further supports the possibility that GABA_A receptors are involved in the responses of SCN neurons to GABA.

The experimentally determined reversal potential of the GABA response depends on $[Cl^-]_p$ (Fig. 3c, d), but is independent of the time of day ($P > 0.4$; Fig. 3f) for any given $[Cl^-]_p$. At 2 mM, an average reversal potential of -60 ± 5 mV ($n = 18$) was calculated for day and night animals. By contrast, a reversal potential of -31 ± 5 mV ($n = 22$) was calculated for $[Cl^-]_p$ of 25 mM. The difference in the measured reversal potential (29 mV) is smaller than expected from a 12.5-times change in $[Cl^-]_p$ (~ 60 mV). This difference is due partly to the permeability of bicarbonate and partly to the large influx of chloride during GABA application under low-chloride-concentration conditions²⁴. The absence of diurnal changes in measured reversal potential is related to the fact that in the whole-cell patch technique the intracellular ion composition is determined by the content of the patch pipette. Thus, by using the whole-cell patch technique we have overridden the endogenous

variations in cytoplasmic composition that occurred during the diurnal cycle.

An excitatory effect of GABA is often found in immature neurons of various origins^{25,26}, and has also been demonstrated in some mature neurons²⁷. The usual explanation for this phenomenon is reversal of chloride gradients, although bicarbonate permeability of the GABA_A channel and altered GABA receptors have also been suggested.

The hypothesis emerging from our results is that high intracellular chloride concentration ($[Cl^-]_i$) during the day induces an excitatory response to GABA, whereas low $[Cl^-]_i$ at night results in an inhibitory response. We tested this under conditions that enabled a glimpse of the original intracellular chloride concentration. These conditions exist during the first few seconds after breaking the cell membrane. Most of the spontaneous synaptic potentials recorded from SCN neurons are blocked by bicuculline (Fig. 4a, b) and have a reversal potential of about -30 mV (Fig. 4d; mean 31 ± 6 mV, $n = 5$; $[Cl^-]_p = 25$ mM), which is similar ($P > 0.5$, paired *t*-test) to the reversal potential of the GABA response (Fig. 4e). Both reversal potentials depend on the chloride concentration gradient. Thus, the change in amplitude of the spontaneous synaptic potentials that occurs after breaking the cell membrane should reflect the change in

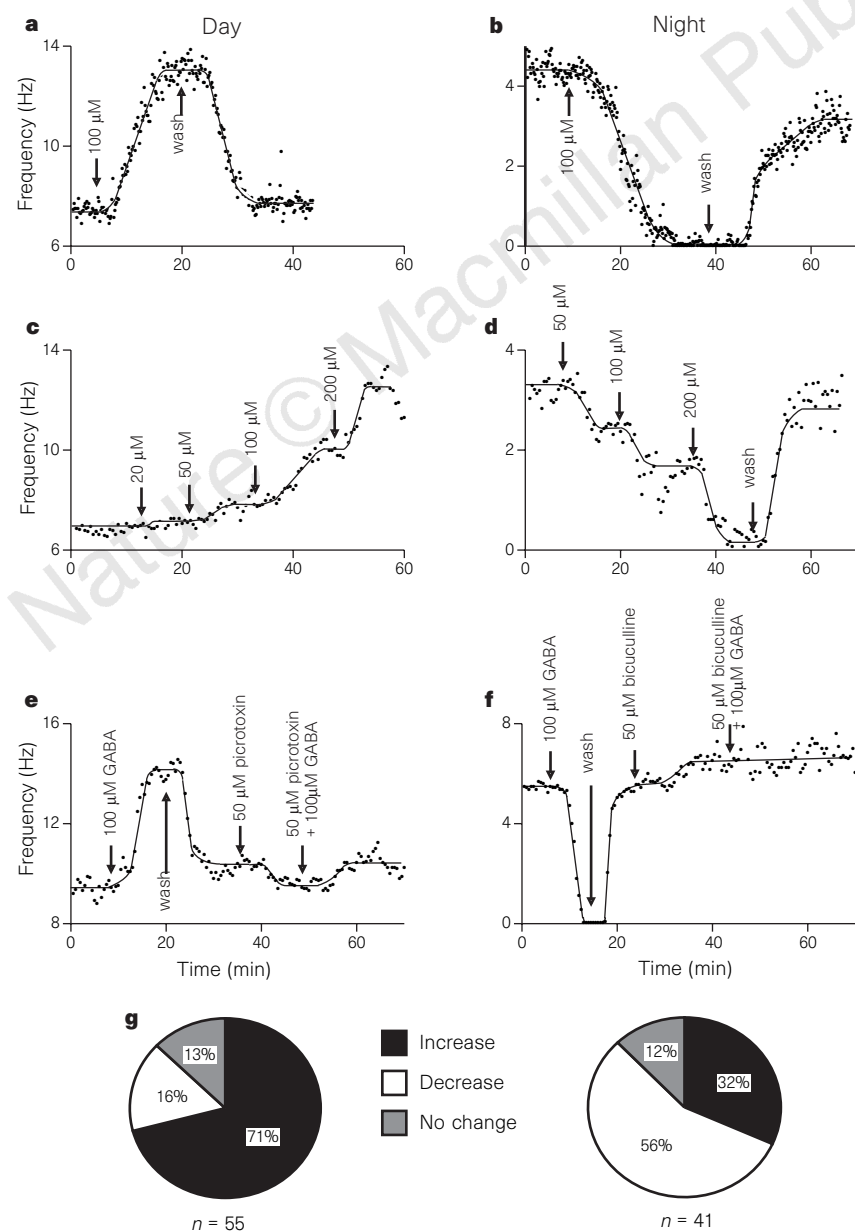


Figure 2 GABA acts as an excitatory neurotransmitter during the day and as an inhibitory neurotransmitter at night. The data are presented in the form of firing rate as a function of time. **a, b**, Time course of the increase (**a**) and the decrease (**b**) in firing rate of SCN neuron in response to GABA (100 μ M) application during day and night, respectively. Each point represents the mean frequency calculated over 30 s. Times for changing solutions and concentrations are marked on the plots. The continuous lines were drawn by hand to emphasize the time course of the changes. **c, d**, both the excitatory (**c**) and inhibitory (**d**) responses to GABA are dose-dependent. **e, f**, Both excitation and inhibition are blocked by picrotoxin or bicuculline. Note that in the presence of blocker, 100 μ M GABA did not alter the firing rate of the neuron. **g**, Distribution of the neuronal responses to GABA during day and night. The response was calculated at steady-state conditions over a period of at least 5 min.

$[Cl^-]_i$ caused by equilibration with the electrode content. To analyse these changes quantitatively, we used the standard deviation (s.d.) of the membrane voltage. As shown in Fig. 4c, the variation in membrane potential, which mainly reflects synaptic activity, decreased with membrane depolarization. The dependence of the s.d. on the membrane potential (Fig. 4d, circles), matched that of synaptic activity amplitude (Fig. 4d, squares). This indicates the validity of using the s.d. as representative of the amplitude of synaptic events.

With 2 mM chloride in the patch pipette, the amplitude of the synaptic potentials and the s.d. of the membrane voltage decreased significantly during the first few seconds after breaking the cell membrane (Fig. 5a), indicating that the original $[Cl^-]_i$ was higher

than 2 mM. However, with 25 mM chloride in the pipette, an increase in the amplitude of the synaptic potentials was invariably observed (Fig. 5b), indicating that the original $[Cl^-]_i$ was lower than 25 mM. Using the s.d. analysis, the changes in amplitude of the spontaneous synaptic potentials were estimated and compared at various times of the day with $[Cl^-]_p = 15$ mM. The amplitude of the synaptic activity decreased (Fig. 5d) in 70% of the neurons from day animals (Fig. 4e). By contrast, an increase in amplitude of synaptic potentials (Fig. 5c) was observed in most (53%) of the neurons from night animals (Fig. 5e). Thus, it appears that during the day the intracellular chloride concentration in most of SCN neurons is higher than 15 mM, whereas during the night it is lower than 15 mM. The different distributions of neurons according to the

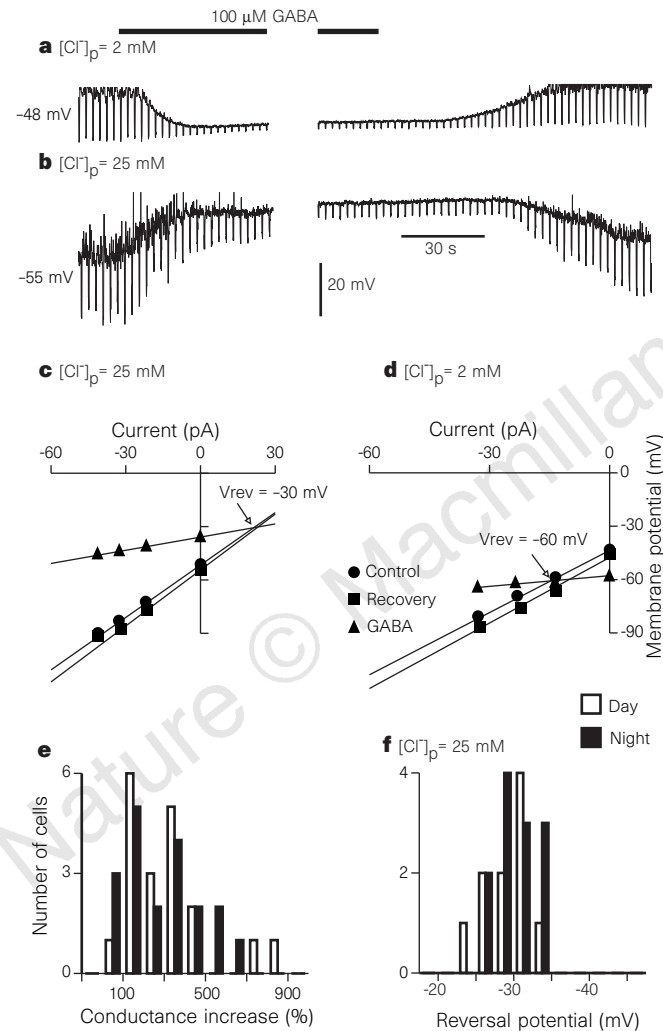


Figure 3 Neither the conductance change nor the reversal potential of the GABA response depend on the time of the day when the whole-cell patch technique was used. **a, b**, The membrane potential and the voltage response to hyperpolarizing current pulses (10 pA), before, during (bar) and after GABA application in day animals. The intracellular solution ($[Cl^-]_p$) contained 2 mM and 25 mM chloride in **a** and **b** respectively. The resting potential is indicated on the left of the traces. Action potentials in **a** were truncated. **c, d**, Current-voltage relationships, from the same experiments as in **b** and **a**, respectively, before (circles), during (triangles) and after (squares) GABA application. The change in slope and the intersection of the lines were used to calculate the conductance change and the reversal potential (V_{rev}) correspondingly. **e, f**, Distribution of the conductance change and reversal potentials of the GABA response, during day (white bars) and night (black bars). The reversal potential was calculated from experiments in which 25 mM of $[Cl^-]_p$ was used and conductance changes were calculated for all experiments.

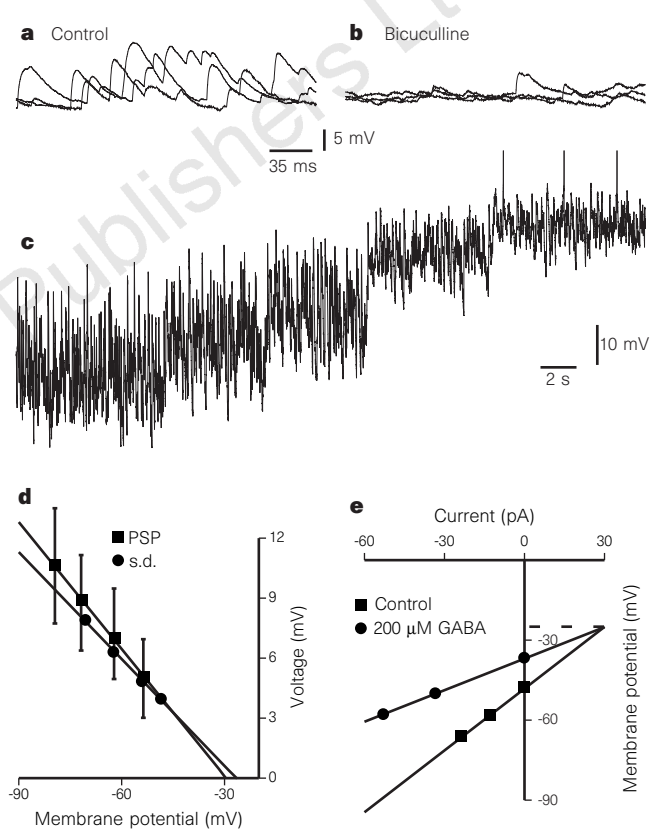


Figure 4 Most of the spontaneous synaptic potentials are GABAergic, and may be used to estimate the intracellular chloride concentration. **a, b**, Bicuculline (50 μM) blocks most of the spontaneous synaptic potentials. Each panel shows three superimposed traces before addition (**a**) and in the presence (**b**) of bicuculline. **c**, Slow rate recording of the fluctuations in membrane voltage at different membrane potentials. The membrane potential was set by intracellular injection of d.c. current. **d**, Both the standard deviation (s.d.) and the mean amplitude of the postsynaptic potentials (PSP) depend on the membrane potential. A reversal potential of -30 V and -28 mV was calculated, respectively. Bars represent the standard error. **e**, In the same cell, the calculated reversal potential of the GABA response was -28 mV.

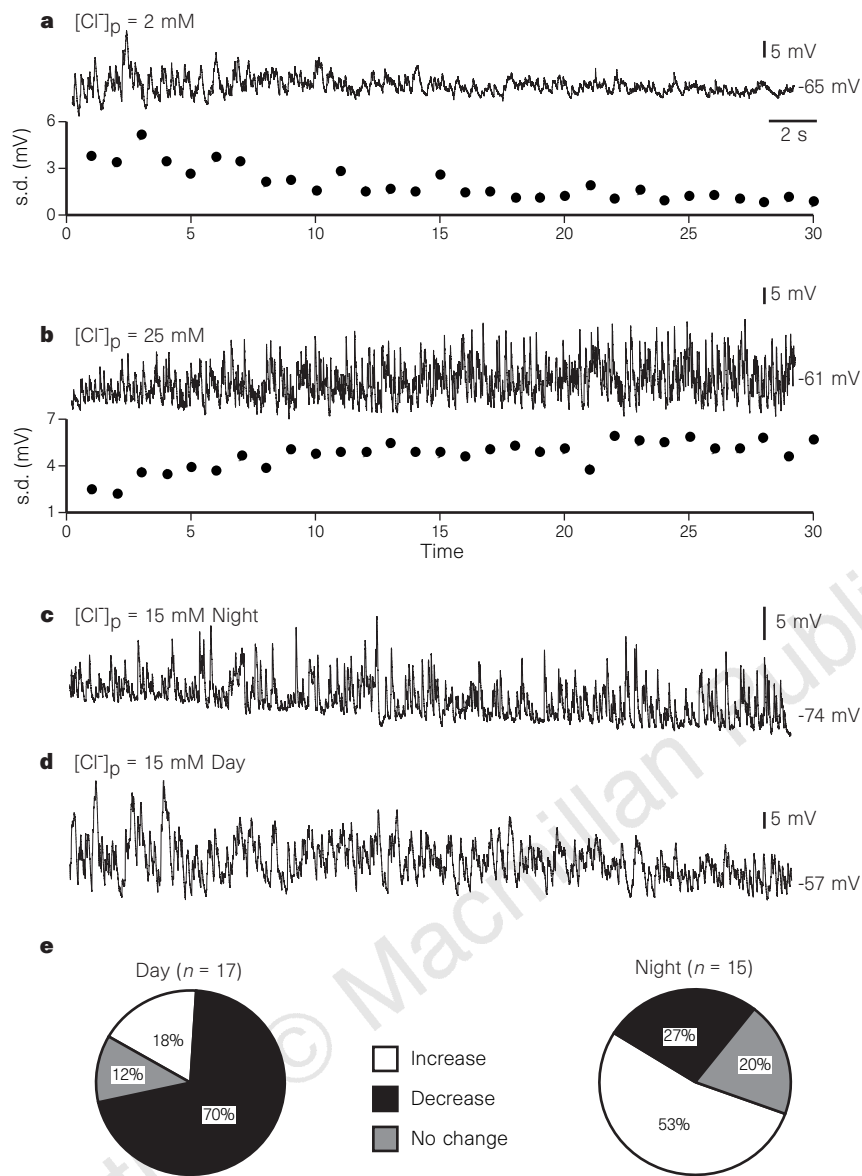


Figure 5 Postulated diurnal alterations in $[Cl^-]_i$, revealed by analysing the amplitude of the spontaneous synaptic potentials. **a**, Upper trace, continuous recordings of membrane potential during the first 30 s after breaking the cell membrane (in day animal). The patch pipette contained 2 mM chloride. Negative d.c. current was injected to prevent firing of the neuron and thus depolarizing synaptic potentials were always recorded. The mean membrane potential is indicated on the right of the trace. Lower trace, standard deviation of the membrane voltage during this period (see Methods). **b**, As in **a**, but for 25 mM chloride. **c, d**, As in **a**, for 15 mM of chloride in night and day animals respectively. **e**, Distribution of neurons according to changes in amplitude of synaptic potentials during the first 40 s after breaking the cell membrane. The patch pipette contained 15 mM chloride. The change in amplitude was calculated from the s.d. of the membrane voltage (see Methods).

calculated change in amplitude of synaptic potentials (Fig. 5e) is similar to that observed for the calculated firing rate (Fig. 2g).

These results indicate that the intracellular chloride concentration in SCN neurons undergoes diurnal oscillations, that is, high concentrations prevail during the day and low concentrations at night. SCN neurons may possess a cyclically modulated ion pump that determines the intracellular chloride concentration. A diurnal oscillation in $[Cl^-]_i$ has two immediate implications. First, with regard to the activity of the SCN's neuronal network, such a process would by itself increase the magnitude of the diurnal changes in firing rate, that is, the dense GABAergic local circuits would act as a positive feedback. At night, when neurons fire at low rates, GABA would act to decrease the firing further, but during the day, when GABA acts as an excitatory agent, the already high firing rate would be augmented. Although a diurnal change in $[Cl^-]_i$ could generate the diurnal variation in firing rate by itself, provided that the neurons are tonically active, it should be noted that isolated neurons exhibit circadian oscillation in firing rate¹³. Second, this new concept, that the intracellular ion composition can be a functional and modifiable physiological factor that governs the excitability of the nervous system, may account for the changes in level of excitability, as well as in susceptibility to epileptic discharge, that are known to occur during specific diurnal periods. □

Methods

Animals and brain slices. For electrophysiological recording fresh brain slices were derived from young (3–8 weeks) Sabra rats that had been entrained to a 12/12 light/dark cycle for at least 2 weeks. Coronal hypothalamic slices (300–500 μm) were prepared as described¹⁰, at zeitgeber time (ZT) 2–4 and ZT 15–17 for day and night experiments, respectively. Following stabilization of the slices in aerated physiological solution, experiments on day animals were performed during ZT 4–9 and on night specimens during ZT 17–21.

Physiology. The physiological solution, aerated with 95% O_2 and 5% CO_2 , was composed of (in mM): NaCl 120; KCl 5; $MgSO_4$ 1.3; KH_2PO_4 1.2; $NaHCO_3$ 26; $CaCl_2$ 2.4; glucose 20. The submerged-slice technique was used throughout. The current of single unit activity was extracellularly recorded by an AXO-PATCH-1D amplifier in the voltage clamp mode at 36 °C. The glass pipette was filled with physiological solution and had a d.c. resistance of 4–8 M Ω . The neurons were randomly sampled from various areas in the SCN and their firing rates were continuously estimated from the average interspike interval calculated every 0.5–2 min. GABA (final concentration, 10–500 μM), bicuculline (20–50 μM) and picrotoxin (50–100 μM) were bath-applied via the physiological solution. The response to GABA was determined by calculating the average firing rate during 5–10 min (~10 independent measurements) of steady-state conditions before and during GABA application. A standard *t*-test was used to estimate the significance of the difference between the measurements

made before and during GABA application. Changes of less than 5% were considered as 'no change', even if the *t*-test showed significance.

The whole-cell patch technique was used for intracellular recordings (AXOCLAMP-2A in current clamp mode at room temperature). The intracellular solution was composed of (in mM): potassium gluconate 120; NaCl 24; CaCl₂ 0.5; Mg-ATP 5; EGTA 5; HEPES 10. The chloride concentration was varied between 2, 15 and 25 mM by replacing the NaCl with sodium gluconate; pH was set to 7.2 with KOH.

The slope of the current-voltage relationship (*I*-*V* curve) was drawn from the voltage response to 250–350 ms negative current pulses of different intensities (10–60 pA). The conductance change in response to GABA application was calculated from the slopes of *I*-*V* curves in the presence or absence of GABA. The intersection point of these curves was used to estimate the reversal potential of the response to GABA (Fig. 3c, d).

The change in amplitude of the synaptic potentials during the first several tens of seconds after breaking the cell membrane was estimated by calculating the s.d. of the membrane voltage, digitized at a rate of 1 kHz, within a time window of 1 s (Figs 4, 5). The s.d. of the first second was compared to the s.d. at steady-state conditions (after at least 40 s). A change of less than 5% was considered as 'no change'.

Morphology. For immuno-ultrastructural observations, adult rats were anaesthetized with intraperitoneal sodium pentobarbital and, following a brief saline wash of the blood system, were perfused with fixative containing 4% glutaraldehyde in 0.1 M sodium cacodylate buffer, pH 7.0. Vibratome sections containing the SCN were post-fixed in 1% osmium tetroxide and 1.5% potassium ferricyanide in 0.05 M cacodylate buffer, and processed for electron microscopy²⁸. On ultrathin sections, post-embedding immunogold labelling was with anti-GABA antibodies (Somogyi code no. 9) and protein-A gold (15 nm) as described²⁸.

Organotypic slice explant cultures of the SCN were derived from neonate (9–12 days) Sabra rats as described¹⁰. After 2–3 weeks *in vitro*, cultures were immersed in fixative containing 4% glutaraldehyde in 0.1 M sodium cacodylate buffer, pH 7.0, before pre-embedding and immunoperoxidase labelling with anti-GABA antibodies. Briefly, following incubation in primary antiserum, cultures were reacted with the avidin-biotinylated peroxidase complex (Vector), and immunoreactivity visualized with diaminobenzidine tetrahydrochloride. Cultures, whole-mounted on subbed slides, were dipped in dilute aqueous osmium tetroxide, dehydrated in ethanol, and coverslipped.

Received 27 September 1996; accepted 19 March 1997.

- Klein, D. C., Moore, R. Y. & Reppert, S. M. (eds) *Suprachiasmatic Nucleus: The Mind's Clock* (Oxford University Press, New York, 1991).
- Myers, M. P. *et al.* Positional cloning and sequence analysis of the *Drosophila* clock gene, *timeless*. *Science* **270**, 805–808 (1995).
- Page, T. L. Time is the essence: Molecular analysis of the biological clock. *Science* **263**, 1570–1572 (1994).
- Moore, R. Y. & Speh, J. C. GABA is the principal neurotransmitter of the circadian system. *Neurosci. Lett.* **150**, 112–116 (1993).
- Buijs, R. M. *et al.* Ultrastructural evidence for intra- and extranuclear projections of GABAergic neurons of the suprachiasmatic nucleus. *J. Comp. Neurol.* **340**, 381–391 (1994).
- Castel, M. *et al.* GABAergic innervation of the mouse suprachiasmatic nucleus. *Eur. J. Neurosci.* (suppl.) **3**, Abstr. 2, 111 (1990).
- Decavel, C. & van den Pol, A. N. GABA: A dominant neurotransmitter in the hypothalamus. *J. Comp. Neurol.* **302**, 1019–1037 (1990).
- Okamura, H. *et al.* Demonstration of GABAergic cell bodies in the suprachiasmatic nucleus: In situ hybridization of glutamic acid decarboxylase (GAD) mRNA and immunocytochemistry of GAD and GABA. *Neurosci. Lett.* **102**, 131–136 (1989).
- Buijs, R. M. *et al.* Colocalization of γ -aminobutyric acid with vasopressin, vasoactive intestinal peptide, and somatostatin in the rat suprachiasmatic nucleus. *J. Comp. Neurol.* **358**, 343–352 (1995).
- Belenky, M. *et al.* The suprachiasmatic nucleus in stationary organotypic culture. *Neuroscience* **70**, 127–143 (1996).
- Strecker, G. J. & Dudek, F. E. Local synaptic circuits in the rat suprachiasmatic nucleus. *Soc. Neurosci. (Abstr.)* **20**, 1439 (1994).
- Strecker, G. J. *et al.* Neurotransmission and electrophysiological mechanisms in the suprachiasmatic nucleus. *Sem. Neurosci.* **7**, 43–51 (1995).
- Welsh, D. K. *et al.* Individual neurons dissociated from rat suprachiasmatic nucleus express independently phased circadian firing rhythms. *Neuron* **14**, 697–706 (1995).
- Ralph, M. R. & Menaker, M. GABA regulation of circadian responses to light. I. Involvement of GABA_A, benzodiazepine and GABA_B receptors. *J. Neurosci.* **9**, 2858–2865 (1989).
- Smith, R. D. *et al.* Bicyuculline and picrotoxin block phase advances induced by GABA agonists in the circadian rhythm of locomotor activity in the golden hamster by a phallofen-insensitive mechanism. *Brain Res.* **530**, 275–282 (1990).
- Collinge, J. *et al.* Prion protein is necessary for normal synaptic function. *Nature* **370**, 295–297 (1994).
- Tobler, I. *et al.* Altered circadian activity and sleep in mice devoid of prion protein. *Nature* **380**, 639–642 (1996).
- Estibeiro, J. P. Multiple roles for PrP in the prion diseases. *Trends Neurosci.* **19**, 257–258 (1996).
- Prosser, R. A. & Gillette, M. U. The mammalian circadian clock in the suprachiasmatic nucleus is reset *in vitro* by cAMP. *J. Neurosci.* **9**, 1073–1081 (1989).

- Gillette, M. U. in *Suprachiasmatic Nucleus: The Mind's Clock* (eds Klein, D. C., Moore, R. Y. & Reppert, S. M.) 125–143 (Oxford University Press, New York, 1991).
- Mason, R. *et al.* The effects of GABA and benzodiazepines on neurones in the suprachiasmatic nucleus (SCN) of Syrian hamsters. *Brain Res.* **552**, 53–57 (1991).
- Bos, N. P. A. & Mirmiran, M. Effects of excitatory and inhibitory amino acids on neuronal discharges in the cultured suprachiasmatic nucleus. *Brain Res. Bull.* **31**, 67–72 (1993).
- Liou, S. Y. & Albers, H. E. Single unit response of neurons within the hamster suprachiasmatic nucleus to GABA and low chloride perfusate during the day and night. *Brain Res. Bull.* **25**, 93–98 (1990).
- Staley, K. J. *et al.* Ionic mechanisms of neuronal excitation by inhibitory GABA_A receptors. *Science* **269**, 977–980 (1995).
- Cherubini, E. *et al.* GABA: an excitatory transmitter in early postnatal life. *Trends Neurosci.* **14**, 515–519 (1991).
- Obrietan, K. & van den Pol, A. N. GABA neurotransmission in the hypothalamus: developmental reversal from Ca²⁺ elevating to depressing. *J. Neurosci.* **15**, 5065–5077 (1995).
- Andersen, P. *et al.* Two different responses of hippocampal pyramidal cells to application of γ -aminobutyric acid. *J. Physiol. (Lond.)* **305**, 279–296 (1980).
- Castel, M. *et al.* Glutamate-like immunoreactivity in retinal terminals of the mouse suprachiasmatic nucleus. *Eur. J. Neurosci.* **5**, 368–381 (1993).

Acknowledgements. We thank M. Belenky for perfecting the organotypic slice explant culture technique; H. Matzner and S. Cohen for technical assistance; and J. Morris for critical reading of the text. Research was supported by the USA–Israel Binational Science Foundation and the Israel Ministry of Science and Technology.

Correspondence and requests for materials should be addressed to S.W. (e-mail: shlomow@lobster.l.s.huji.ac.il).

The *Rx* homeobox gene is essential for vertebrate eye development

P. H. Mathers[†], A. Grinberg[‡], K. A. Mahon[§] & M. Jamrich*

* Laboratory of Developmental Biology, Food and Drug Administration, Rockville, Maryland 20852, USA

‡ Laboratory of Mammalian Genes and Development, NICHD, NIH, Bethesda, Maryland 20892, USA

§ Department of Cell Biology, Baylor College of Medicine, Houston, Texas 77030, USA

Development of the vertebrate eye requires a series of steps including specification of the anterior neural plate, evagination of the optic vesicles from the ventral forebrain, and the cellular differentiation of the lens and retina. Homeobox-containing genes, especially the transcription regulator *Pax6*, play a critical role in vertebrate and invertebrate eye formation. Mutations in *Pax6* function result in eye malformations known as *Aniridia* in humans and *Small eye* syndrome in mice^{1–3}. The *Drosophila* homologue of *Pax6*, *eyeless*, is also necessary for correct invertebrate eye development, and its misexpression leads to formation of ectopic eyes in *Drosophila*^{4,5}. Here we show that a conserved vertebrate homeobox gene, *Rx*, is essential for normal eye development, and that its misexpression has profound effects on eye morphology. *Xenopus* embryos injected with synthetic *Rx* RNA develop ectopic retinal tissue and display hyperproliferation in the neuroretina. Mouse embryos carrying a null allele of this gene do not form optic cups and so do not develop eyes. The *Rx* gene family plays an important role in the establishment and/or proliferation of retinal progenitor cells.

The *Rx* homeobox genes were first isolated from a cDNA library made from *Xenopus* animal-cap ectoderm induced by treatment with ammonium chloride. This treatment was chosen because it can activate transcription of genes involved in anterior head formation^{6–8}. The predicted amino-acid sequence of the *Xenopus Rx* genes shows that each gene contains a highly conserved paired-like homeodomain⁹ and octapeptide¹⁰ typical of this homeobox gene subfamily (Fig. 1a). They also contain a conserved motif in the carboxy-terminal end of their proteins. This domain is present in several paired-like homeobox genes, and the consensus sequence of

[†] Present address: Departments of Otolaryngology and Biochemistry, West Virginia University School of Medicine, Morgantown, West Virginia 26506, USA